ACS APPLIED MATERIALS & INTERFACES

Research Article

www.acsami.org

An Iron-based Film for Highly Efficient Electrocatalytic Oxygen Evolution from Neutral Aqueous Solution

Mingxing Chen,[†] Yizhen Wu,[†] Yongzhen Han,[†] Xiaohuan Lin,[§] Junliang Sun,[§] Wei Zhang,*[,‡] and Rui Cao*[,†,‡]

[†]Department of Chemistry, Renmin University of China, Beijing 100872, China

[‡]School of Chemistry and Chemical Engineering, Shaanxi Normal University, Xi'an 710119, China

[§]College of Chemistry and Molecular Engineering, Peking University, Beijing 100871, China

Supporting Information

ABSTRACT: An ultrathin Fe-based film was prepared by electrodeposition from an Fe^{II} solution through a fast and simple cyclic voltammetry method. The extremely low Fe loading of 12.3 nmol cm^{-2} on indium tin oxide electrodes is crucial for high atom efficiency and transparence of the resulted film. This Fe-based film was shown to be a very efficient electrocatalyst for oxygen evolution from neutral aqueous solution with remarkable activity and stability. In a 34 h controlled potential electrolysis at 1.45 V (vs NHE) and pH 7.0, impressive turnover number of 5.2×10^4 and turnover frequency of 1528 h^{-1} were obtained. To the best of our knowledge, these values represent one of the highest among electrodeposited catalyst films for water oxidation under comparable conditions. The morphology and the composition of the catalyst film was determined by scanning electron microscopy, transmission electron microscopy, energy-dispersive X-ray, and X-ray photoelectron spectroscopy, which all confirmed the deposition of Fe-based materials with Fe^{III} oxidation state on the electrode. This study is significant because of the use of iron, the fast and simple cyclic voltammetry electrodeposition, the extremely low catalyst loading and thus the transparency of the catalyst film, the remarkable activity and stability, and the oxygen evolution in neutral aqueous media.

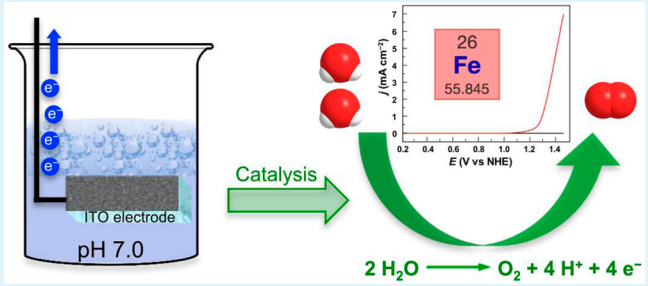

KEYWORDS: *electrocatalysis, iron, film preparation, oxygen evolution, water splitting*

1. INTRODUCTION

Energy and environmental concerns related to the use of fossil fuels have forced people to seek renewable and clean energy resources.[1−4] One promising solution is to use solar energy to split water for hydrogen and oxygen production.[5−7] As one of the half reactions, the oxidation of water to produce O_2 is challenging from both thermodynamic and kinetic points of view, and thus, this process is considered to be the bottleneck for water splitting.[4,7] Extensive efforts have been made recently in identifying molecular complexes and solid materials that are active for electrocatalytic oxygen evolution reaction (OER).[4,8−21] Although complexes and materials made of ruthenium and iridium have been shown to be active to catalyze the oxidation of water,[22−30] the low earth abundance and high cost of these noble metal elements limit their widespread applications. It is therefore extremely desirable to find low-cost, active, and robust catalysts for water oxidation.

Metal oxides,[31−42] hydroxides,[43−45] and oxyhydroxides[46−49] of earth-abundant iron group elements (i.e., iron, cobalt, and nickel) have been generally acknowledged to be one of the most competent candidates as OER catalysts. Despite these achievements, however, substantial improvements in the design and preparation of OER catalysts of iron group elements are still needed, particularly in the following two subjects. First, few OER catalysts operate in neutral aqueous media. Typically, concentrated basic solutions are required for the aforesaid catalysts to show satisfactory OER activity and stability.[10,20,34−36] For example, we recently demonstrated that a Ni-based catalyst film deposited on electrodes retained its OER activity in basic solutions but quickly deactivated at neutral pH, probably due to the dissolution of the Ni-based material during electrocatalysis under conditions of insufficient bases.[50] Because basic solutions are corrosive and are not environmentally benign, their uses are restricted. As a result, OER catalysts that are effective and stable in neutral aqueous solution are preferred.

Second, Fe-based electrocatalysts for water oxidation have been much less explored as compared to Co and Ni,[51] which is in a sharp contrast to the fact that Fe has very rich redox properties for O_2 activation in both biological and biomimetic systems.[52,53] In addition, Fe is more earth abundant and cheaper and is less toxic than the other two iron group

Received: July 10, 2015
Accepted: September 14, 2015
Published: September 14, 2015

DOI: 10.1021/acsami.5b06195
ACS Appl. Mater. Interfaces 2015, 7, 21852−21859

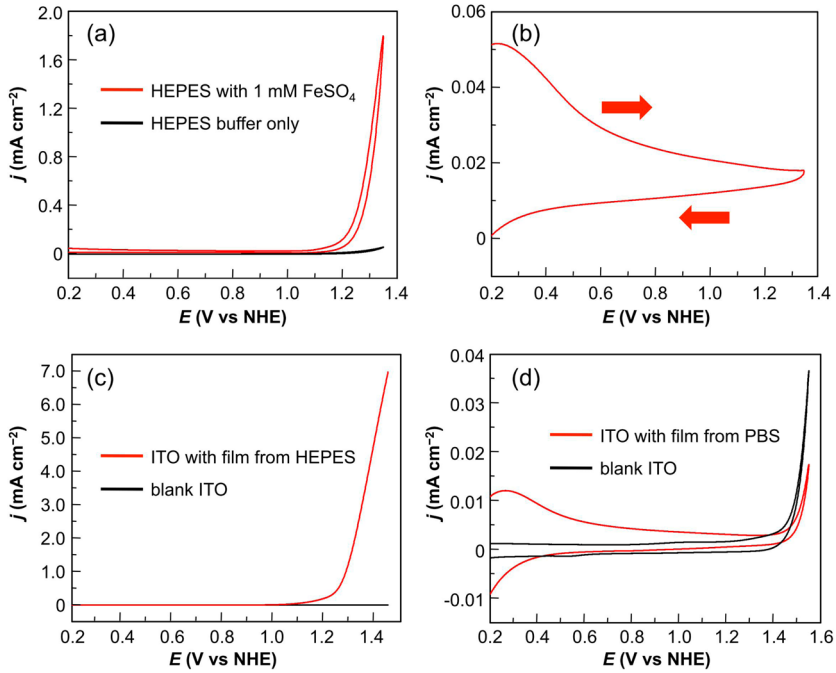

Figure 1. (a) CVs of ITO electrodes in 0.1 M pH 7.0 HEPES buffer with and without 1.0 mM of $FeSO_4$. (b) CV of an ITO electrode in 0.1 M pH 7.0 phosphate buffer with 1.0 mM of $FeSO_4$. (c) LSV of blank and catalyst-coated ITO in 0.1 M pH 7.0 phosphate buffer. The catalyst-coated ITO was obtained by electrodeposition from a 1.0 mM of Fe^{II} in 0.1 M pH 7.0 HEPES buffer via 5 CV cycles of 0.20 to 1.35 V at 50 mV s^{-1} scan rate. (d) CVs of blank and pretreated ITO in 0.1 M pH 7.0 phosphate buffer. The pretreated ITO was obtained in a similar way as in c except the use of PBS buffer. Conditions: scan rate 50 mV s^{-1}, 20 °C.

elements. One possible reason for the lack of studies on Fe-based electrocatalysts may be the difficulty for the preparation of Fe-based catalyst films via electrodeposition, which is a generally employed method to prepare Co- and Ni-based catalyst films onto electrodes.[9,10,35,54−56] It is known that the solubility of Fe^{III} in neutral or basic aqueous solutions is extremely low, which challenges the electrodeposition from Fe^{III} solutions. Although there are many kinds of preparation methods, such as dip-coating,[57] spin-coating,[58] aerosol spray,[59] template synthesis,[60] and solid state reaction,[61] electrodeposition is a simple, convenient, energy-saving, and efficient method used to prepare catalyst films onto a variety of large-surface electrodes.[62] Therefore, the development of highly active and robust Fe-based OER catalyst films via electrochemical routines remains a fundamental challenge.

Herein, we report the preparation of an Fe-based film by electrodeposition from an Fe^{II} solution and its remarkable electrocatalytic performance for OER in neutral aqueous media. This film was prepared by cyclic voltammetry (CV) method. The ultrathin and transparent film has an extremely low Fe loading of 12.3 nmol cm^{-2}. In a 34 h electrolysis in pH 7.0 aqueous solution with a constant applied potential of 1.45 V vs normal hydrogen electrode (NHE; all potentials reported in this work are referenced to NHE), impressive turnover number (TON) 5.2×10^4 and turnover frequency (TOF) 1528 h^{-1} were obtained. Characterization of this film material by scanning electron microscopy (SEM), transmission electron microscopy (TEM), energy-dispersive X-ray (EDX) and X-ray photoelectron spectroscopy (XPS) confirmed the deposition of Fe-based materials with Fe^{III} oxidation state on the electrode. This study is significant in several aspects, including the use of iron, the fast and simple CV electrodeposition, the ultrathin and transparent film with an extremely low catalyst loading, the remarkable activity and stability, and the oxygen evolution in neutral aqueous media.

2. RESULTS AND DISCUSSION

2.1. Preparation of Fe-based Film. Because Fe^{III} ions have very limited solubility in neutral buffer solutions, Fe^{II} ions are chosen in this study as an iron source for film deposition. We first tried to prepare Fe-based films via electrodeposition onto indium tin oxide (ITO) electrodes from a 0.1 M pH 7.0 phosphate buffer solution (PBS). However, precipitation happened immediately upon the addition of $FeSO_4$, which obviously challenged the preparation of Fe-based films. As shown in Figure 1b, CV of this slurry solution for film deposition displayed small currents even scanning to 1.35 V, which indicated the absence of active catalyst films that may possibly be deposited onto the electrode. After this treatment, the ITO electrode was taken out, gently rinsed with deionized water, and was then examined in an Fe-free 0.1 M pH 7.0 phosphate buffer. As we expected, CV of such pretreated electrodes showed even smaller OER current densities as compared to blank ITO electrodes, probably due to the poor electrical conductivity of the precipitated materials covered on the electrode surfaces (Figure 1d).

The use of electrolytes such as sulfate, nitrate, and perchlorate that are commonly used in electrochemistry gave no obvious film deposition due to their lack of proton-accepting properties.[63] The use of buffer anions that can accept protons is necessary for successful film electrodeposition, because proton-accepting anions are able to keep a stable local pH environment by taking the protons released from water molecules during the deposition of metal oxide or hydroxide films.[63] It is known that protons accumulate at the working electrode when metal oxides or hydroxides are forming. In the absence of proton acceptors,

DOI: 10.1021/acsami.5b06195
ACS Appl. Mater. Interfaces 2015, 7, 21852−21859

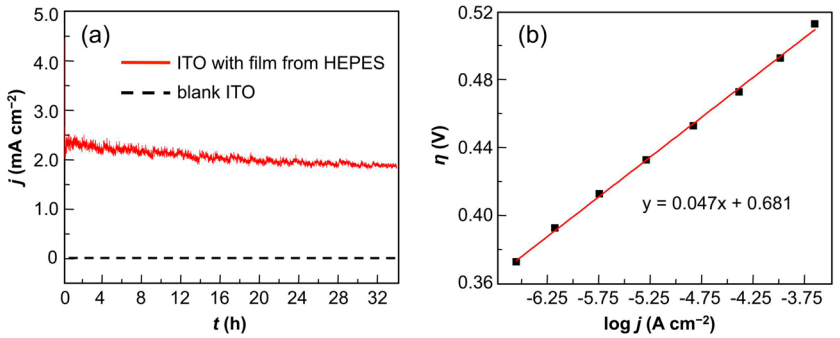

Figure 2. (a) Current curves of CPE at 1.45 V in 0.10 M pH 7.0 phosphate buffer using blank or catalyst-coated ITO electrodes. The Fe-based film was electrodeposited from 0.1 M pH 7.0 HEPES buffer containing 1.0 mM $FeSO_4$ with 5 CV cycles between 0.20 and 1.35 V at 50 mV s^{-1} scan rate. (b) Tafel plot, $\eta = E_{appl} - iR - E_0$, of the Fe-based film from HEPES in 0.1 M phosphate buffer (pH 7.0). In this equation, E_{appl} is the applied potential, and E_0 = 0.82 V is the thermodynamic potential for water oxidation at pH 7.0. The slope is 47 mV per decade.

deposited metal oxides or hydroxides will corrode. As a result, the presence of proton-accepting anions is crucial to the film formation process. Similarly, borate buffer solutions were not used in this work for film deposition due to the insufficient buffering capacities of borate anions at neutral pH.

Due to the above-mentioned reasons, we decided to choose sulfonate-based *N*-(2-hydroxyethyl)piperazine-*N*′-(2-ethanesulfonate) (HEPES) buffer solution for the electrodeposition of Fe-based films. Before the dissolution of $FeSO_4$, the 0.1 M pH 7.0 HEPES buffer was thoroughly purged with nitrogen gas for at least 30 min to remove dissolved oxygen. This treatment is essential because Fe^{II} can be oxidized to Fe^{III} by O_2 that is dissolved in aqueous solution. The resulted Fe^{III} ions will be precipitated as $Fe(OH)_3$ (K_{sp} = 2.6 × 10^{-39}) prior to the electrodeposition, and $Fe(OH)_3$ is known to have low electrical conductivity and thus to adversely affect the efficient electron transfer on electrode surfaces. After dissolution, the film was prepared by electrodeposition on ITO electrodes. The CV of 1.0 mM of Fe^{II} displayed a pronounced catalytic wave with an onset at about 1.16 V (Figure 1a). Unless otherwise noted, compensated cell resistance (*iR*) was accounted for all CVs. Importantly, there was no such anodic wave observed in the HEPES buffer alone under identical conditions. The successive CVs were almost identical to the first CV cycle (Figure S1). The observation of a pronounced catalytic wave in the CV of an Fe^{II} HEPES buffer is a strong evidence for the formation and deposition of an Fe-based film that is active for electrocatalytic water oxidation.

2.2. Electrocatalytic OER Activity of Fe-based Film. After electrodeposition, the ITO electrode was removed from the HEPES buffer and gently rinsed with deionized water. Its catalytic performance was then examined in an Fe-free 0.1 M pH 7.0 phosphate buffer. Linear sweep voltammetry (LSV) of this catalyst-loaded electrode displayed a strong catalytic wave of 7.0 mA cm^{-2} at 1.45 V, which corresponds to an overpotential (η) of 630 mV (Figure 1c). The onset of this catalytic wave was at 1.29 V (measured at current density j = 1.0 mA cm^{-2}). The OER activity of several well-known catalyst systems based on earth-abundant transition metal elements in neutral aqueous solution[9,14,57,64−70] is summarized in Table S1. Importantly, no further treatments, such as aging, annealing or anodic oxidation, were needed to reach this high activity with the as-prepared catalyst film. The strong anodic wave was attributed to the catalytic oxidation of water to O_2, as large amounts of gas bubbles were observed on the electrode surface. This result is noteworthy because the development of efficient OER catalysts that are active in neutral aqueous solutions is the key for large-scale applications.

The electrocatalytic performance of this Fe-based film was further examined in controlled potential electrolysis (CPE) experiments. Electrolysis was carried out in 0.1 M pH 7.0 phosphate buffer in a two-compartment cell with an applied potential of 1.45 V (η = 630 mV). As shown in Figure 2a, the current density maintained above 1.80 mA cm^{-2} in a 34 h electrolysis with the deposited Fe-based film. The slight current decrease was caused by pH decrease during electrolysis according to eq 1.

$$2H_2O \rightarrow O_2 + 4H^+ + 4e^- \quad (1)$$

After 34 h of CPE, the measured pH value was 6.35. Significantly, the electrolysis current could be recovered if the pH was adjusted back to 7.0 with the addition of NaOH. Current density of <30 μA cm^{-2} was observed in control experiments using blank ITO electrodes. These results showed that this Fe-based film was highly active and robust in prolonged CPE measurements in neutral aqueous solution. During electrolysis, a large amount of O_2 bubbles was observed, and the amount of evolved O_2 was quantitatively determined by gas chromatography, which gave a Faradaic yield of >98%.

The amount of Fe-based catalyst deposited on the ITO electrode was carefully determined by using inductively coupled plasma atomic emission spectroscopy (ICP-AES). After electrodeposition from a 1.0 mM of Fe^{II} in 0.1 M pH 7.0 HEPES buffer via 5 CV cycles of 0.20−1.35 V at 50 mV s^{-1} scan rate, the ITO electrode was taken out from the solution, gently washed with deionized water, and the deposited catalyst film was then dissolved in 0.1 M HNO_3. The resulted solution was subjected to ICP-AES analysis, which gave an extremely low Fe loading of 12.3 nmol cm^{-2} (see the Experimental Section for details). This number corresponds to 18 Fe atoms per 25 $Å^2$ and indicates the formation of averagely a three-atom-layer film on the electrode.[10] Due to the extremely low catalyst loading, the deposited film was transparent (Figure S2). This feature is important, as transparent catalyst films are ideal to be employed in devices for solar cells and photocatalytic water splitting.[71,72]

With this information, we can calculate the TON of 5.2 × 10^4 in a 34 h electrolysis at pH 7.0 under 1.45 V applied potential, and the TOF was 1528 h^{-1} per deposited Fe ion. The TOF value of this Fe-based film is extraordinary as compared to many other catalyst films of Mn, Co, and Ni, and represents one of the highest among electrodeposited OER catalyst films.

DOI: 10.1021/acsami.5b06195
ACS Appl. Mater. Interfaces 2015, 7, 21852−21859

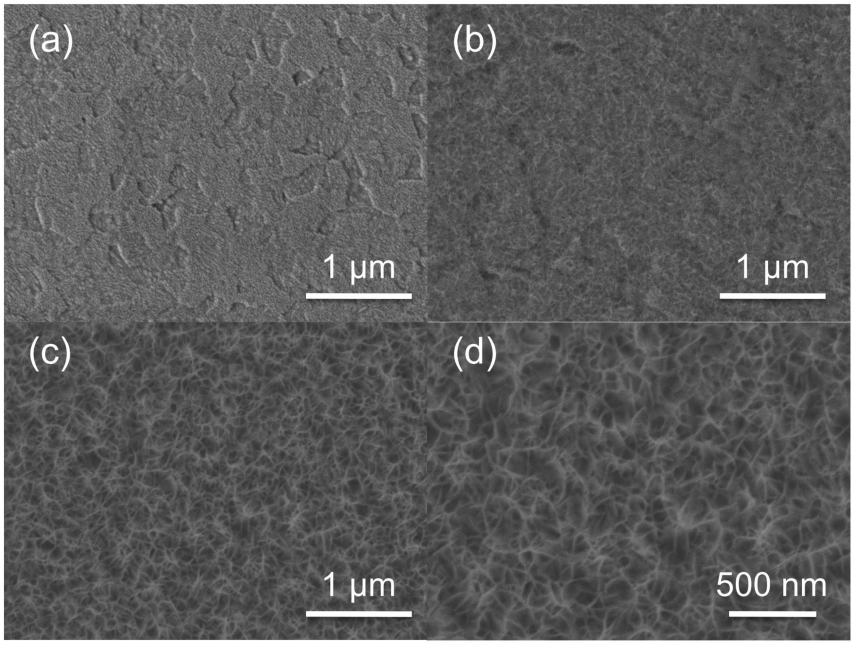

Figure 3. SEM images of (a) blank and (b–d) catalyst-coated ITO electrodes. The Fe-based film was electrodeposited from 0.1 M pH 7.0 HEPES buffer containing 1.0 mM $FeSO_4$ via different CV cycles between 0.20 and 1.35 V at 50 mV s^{-1} scan rate; (b) 5 cycles and (c and d) 50 cycles.

It is necessary to note that the use of concentrated alkaline solution and/or different electrodes, such as gold and nickel foam substrates, is expected to lead to considerably enhanced activity for electrocatalytic water oxidation.[20,47,49,59,73−75] Therefore, the evaluation of OER activity should be carried out under comparable conditions. In addition, all Fe ions were assumed to participate in the OER catalysis in our TOF calculation. As the number of active sites is expected to be only a fraction of the number of Fe ions, a lower limit of the TOF was obtained for the Fe-based catalyst film. In addition to prolonged CPE test, the robustness of this Fe-based catalyst film was further examined by an accelerated durability test (ADT).[76−80] The ADT was carried out with CV cycling between 0.20 to 1.45 V at 500 mV s^{-1} scan rate. As shown in Figure S7, the electrochemical behaviors of the catalyst film on an ITO electrode before and after 500 ADT cycles were almost unchanged, which indicated its stability during OER. The Tafel plot, which provides the relationship between the rate of an electrochemical reaction and the overpotential, was also determined in 0.1 M pH 7.0 phosphate buffer (Figure 2b). The Tafel slope of this Fe-based film is 47 mV per decade, which is also an evidence for its great performance in electrocatalytic OER (Table S1).

2.3. Characterization of Fe-based Film. The morphology of the Fe-based catalyst film was analyzed by SEM. As shown in Figure 3, the film was composed of slender strips, which showed the structure of rippled nanosheets. SEM studies revealed that these strips became longer and thicker with more cycles of CV deposition. After 50 CV cycles, the ITO electrode surface was completely covered by such strips (Figure 3c,d). These strips interconnected to form macroporous film nanostructures. This morphology expands the surface area for water oxidation. TEM suggested a layered structure morphology for the electrodeposited film scraped from the ITO electrode (Figure 4a,b), and high-resolution TEM (HRTEM) showed that this film is a polycrystalline material with many crystallites of varying sizes (ca. 5 nm) and orientations (Figure 4c,d).

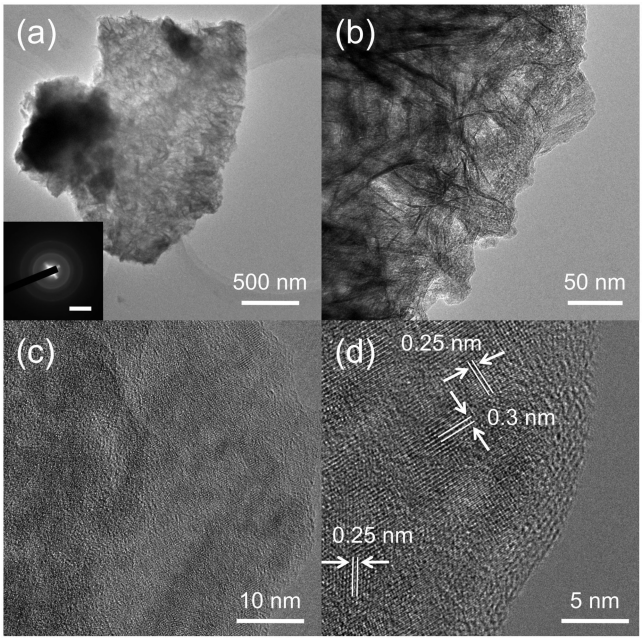

Figure 4. (a and b) TEM and (c and d) HRTEM images of the Fe-based film sample scraped from the ITO electrode. (a, inset) Selected-area electron diffraction (SAED) pattern of the aggregates with a 5 nm^{-1} scale bar.

The composition of the catalyst film was determined by EDX (Figure S3) and XPS (Figure 5 and Figure S4), which all confirmed the deposition of Fe-based materials on the ITO electrode. The XPS spectrum of a blank ITO electrode was shown in Figure S8. No Fe signals but sharp peaks of In $3p_{1/2}$ and Sn $3p_{3/2}$ were observed around the Fe 2p energy region from a blank ITO electrode. The XPS spectrum of the Fe 2p

DOI: 10.1021/acsami.5b06195
ACS Appl. Mater. Interfaces 2015, 7, 21852−21859

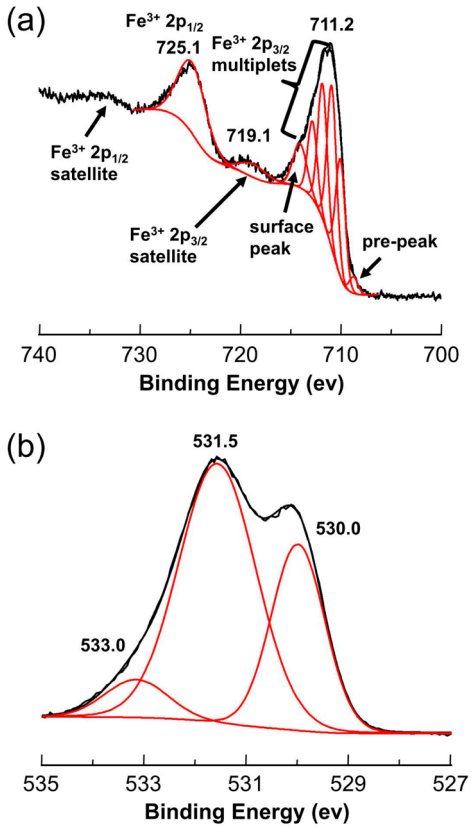

Figure 5. XPS spectrum around the (a) Fe 2p and (b) O 1s energy regions.

energy region from the electrodeposited film indicated Fe^{III} oxidation state based on the established method (Figure 5a).[81] First, the spectrum can be well fitted to show characteristic multiplets and surface peak for Fe^{III} $2p_{3/2}$. Second, the 7.9 eV peak splitting between the envelope (711.2 eV) and the satellite (719.1 eV) of Fe $2p_{3/2}$ was consistent with the Fe^{III} oxidation state (for Fe^{II}, this value was around 5 eV). The XPS spectrum of the O 1s energy region was also resolved (Figure 5b). The three subpeaks with binding energy (BE) at 530.0, 531.5, and 533.2 eV were assigned to oxygen atoms of oxide and hydroxide groups and to water molecules, respectively. The catalyst film was further characterized by UV−vis and Raman spectroscopy (Figure S5 and S6), and these results were consistent with the formation of an Fe-based material on the electrode.

3. EXPERIMENTAL SECTION

3.1. General Materials and Instruments. All chemical reagents, including $FeSO_4{\cdot}7H_2O$ (99.999%, Alfa), $NaH_2PO_4{\cdot}2H_2O$ (99.99%, Alfa), Na_2HPO_4 (99.99%, Alfa), HEPES (99%, Acros), $NaOAc{\cdot}3H_2O$ (99.5%, Acros) and HOAc (99.8%, Acros) were purchased from commercial suppliers and were used without further purification. Milli-Q water of 18 MΩ cm was used in all experiments. UV−visible absorption spectra were acquired on U-3900 spectrophotometer using a standard accessory instead of the square cell holder to fixate ITO electrodes. Two blank ITO electrodes were first inserted into the accessory for baseline correction, and then one was replaced by an ITO electrode electrodeposited with catalyst film via 5 CV cycles. Wavelength was set from 240 to 800 nm, and scan speed was 300 nm/min. Raman spectra of catalyst films were measured by HR-800 with a He−Ne laser, whose wavelength was at 633 nm. To make sure enough catalyst loading for test, catalyst film was electrodeposited onto a 1.0 cm^2 ITO electrode via 200 CV cycles. SEM images were obtained using JSM 7401F. After electrodeposition, film-coated ITO electrodes were taken out, rinsed with deionized water and dried in air before being loaded into the instrument. Images were obtained with an acceleration voltage of 3−5 kV. TEM, HRTEM images, SAED patterns, and EDX spectra were obtained using JEM-2100F(UHR). After electrodeposition of Fe-based films onto ITO of 10.0 cm^2 via 5 CV cycles, the ITO electrodes were rinsed gently with deionized water and dried in air, and then the deposited material was carefully scraped off. The combined material was dispersed in absolute ethanol by ultrasound, and a drop of the mixture was dried on a carbon-coated copper grid for analysis. The amount of loaded Fe after electrodeposition via 5 CV cycles was ascertained by ICP-AES using VISTA-MPX ICP-AES. The Fe-based film formed on 6.0 cm^2 ITO via 5 CV cycles was dissolved in 5.0 mL of 0.1 M HNO_3. The Fe concentration of 0.82 mg/L was obtained using the working curve method, which suggested that 12.3 nmol of Fe was electrodeposited onto 1.0 cm^2 of ITO electrode. XPS was performed on ThermoFisher ESCALab 250Xi using 200 W monochromated Al Kα radiation. The 500 μm X-ray spot was used for XPS analysis. The base pressure in the analysis chamber was about 3×10^{-10} mbar. Typically the hydrocarbon C 1s line at 284.6 eV from adventitious carbon is used for energy referencing. The sample used for XPS was prepared by depositing Fe-based film on ITO via 5 CV cycles between 0.20 and 1.35 V. The survey scan is shown in Figure S4, and the energy regions of Fe 2p and O 1s are shown in Figure 5a,b.

3.2. Electrochemical Studies. All electrochemical experiments were carried out at 20 °C using CH Instruments (model CHI 660D Electrochemical Analyzer). CVs were performed in 15 mL of aqueous solution with a conventional three-electrode configuration: a 0.25 cm^2 ITO working electrode, a saturated Ag/AgCl reference electrode, and a Pt wire auxiliary electrode. All potentials were reported versus NHE through the addition of 0.197 V to the measured potentials. Compensation for *iR* drop was accounted for all CVs. CPE was recorded in 20 mL of 0.10 M pH 7.0 phosphate buffer at 1.45 V in a fritted cell with a 0.25 cm^2 ITO working electrode.

3.3. Formation of Fe-based Films. The Fe-based films were prepared through CV electrodeposition method. A 0.25 cm^2 ITO electrode was used as the working electrode. The deposition solution consisted of 1.0 mM of $FeSO_4$ in 10 mL of 0.1 M pH 7.0 HEPES buffer, and the solution was vigorously bubbled with N_2 for at least 30 min to remove O_2 before the dissolution of $FeSO_4$. The scan rate was 50 mV s^{-1} unless otherwise noted.

3.4. Tafel Plot. Current−potential data were acquired by CPE in 20 mL of 0.1 M pH 7.0 phosphate buffer at a variety of applied potentials in a two-compartment cell. One compartment contained a Pt auxiliary electrode and the other compartment contained the working and Ag/AgCl reference electrodes. The working electrode was prepared by depositing Fe-based film on 0.25 cm^2 ITO via 5 CV cycles between 0.20 and 1.35 V. All data were collected with *iR* compensation. The stable currents were measured at applied potentials ranging from 1.19 to 1.33 V in every 20 mV step for 600-s CPE experiments with the solution being gently stirred. Typically, the current reached a steady state at a particular potential in 2−3 min at every certain potential with currents ranging from 0.32 μA/cm^2 to 0.22 mA/cm^2.

3.5. Characterization of Oxygen Evolution. Analysis of O_2 produced in CPE experiments was conducted by using a gas chromatography (GC-2014C of SHIMADZU) with a gastight electrochemical cell. The experiment was performed in a three-compartment gastight electrochemical cell. The working electrode was prepared by depositing Fe-based film on 1.0 cm^2 ITO via 5 CV cycles between 0.20 and 1.35 V.

4. CONCLUSIONS

In summary, we reported on an Fe-based catalyst film with remarkable activity and stability for electrocatalytic OER in neutral aqueous solution. This film was prepared by a fast and simple CV electrodeposition method, and showed an

DOI: 10.1021/acsami.5b06195
ACS Appl. Mater. Interfaces 2015, 7, 21852−21859

impressive TON of 5.2×10^4 and TOF of 1528 h^{-1} in a 34 h CPE experiment at 1.45 V and pH 7.0. To the best of our knowledge, these values represent one of the highest among electrodeposited OER catalyst films. The extremely low Fe loading of 12.3 nmol cm^{-2} is critical for high atom efficiency and transparency of the resulted catalyst film. The use of iron and the OER in neutral aqueous media is significant, and therefore this study should bring new insights into the preparation of more efficient OER catalysts.

■ ASSOCIATED CONTENT

Supporting Information

The Supporting Information is available free of charge on the ACS Publications website at DOI: 10.1021/acsami.5b06195.

(PDF)

Photography of ITO electrodes, detailed electrochemical measurements, ADT results, XPS, EDX, Raman, and solid-state UV-visible spectra, and a table to compare catalytic performance of different catalysts

■ AUTHOR INFORMATION

Corresponding Authors

*E-mail: ruicao@ruc.edu.cn,
*E-mail: zw@snnu.edu.cn.

Notes

The authors declare no competing financial interest.

■ ACKNOWLEDGMENTS

We thank Professor Qingming Zhang for Raman data collection and helpful discussions. We are grateful for the support from the "Thousand Talents Program" of China, the National Natural Science Foundation of China under grant no. 21101170, the Fundamental Research Funds for the Central Universities, and the Research Funds of Renmin University of China and Shaanxi Normal University.

■ REFERENCES

(1) Grätzel, M. Photoelectrochemical Cells. *Nature* **2001**, *414*, 338–344.

(2) Cook, T. R.; Dogutan, D. K.; Reece, S. Y.; Surendranath, Y.; Teets, T. S.; Nocera, D. G. Solar Energy Supply and Storage for the Legacy and Nonlegacy Worlds. *Chem. Rev.* **2010**, *110*, 6474–6502.

(3) Cao, R.; Lai, W. Z.; Du, P. W. Catalytic Water Oxidation at Single Metal Sites. *Energy Environ. Sci.* **2012**, *5*, 8134–8157.

(4) Kärkäs, M. D.; Verho, O.; Johnston, E. V.; Åkermark, B. Artificial Photosynthesis: Molecular Systems for Catalytic Water Oxidation. *Chem. Rev.* **2014**, *114*, 11863–12001.

(5) Lubitz, W.; Reijerse, E. J.; Messinger, J. Solar Water-Splitting into H_2 and O_2: Design Principles of Photosystem II and Hydrogenases. *Energy Environ. Sci.* **2008**, *1*, 15–31.

(6) Dau, H.; Zaharieva, I. Principles, Efficiency, and Blueprint Character of Solar-Energy Conversion in Photosynthetic Water Oxidation. *Acc. Chem. Res.* **2009**, *42*, 1861–1870.

(7) Nocera, D. G. The Artificial Leaf. *Acc. Chem. Res.* **2012**, *45*, 767–776.

(8) Artero, V.; Chavarot-Kerlidou, M.; Fontecave, M. Splitting Water with Cobalt. *Angew. Chem., Int. Ed.* **2011**, *50*, 7238–7266.

(9) Kanan, M. W.; Nocera, D. G. In Situ Formation of an Oxygen-Evolving Catalyst in Neutral Water Containing Phosphate and Co^{2+}. *Science* **2008**, *321*, 1072–1075.

(10) Dincă, M.; Surendranath, Y.; Nocera, D. G. Nickel-Borate Oxygen-Evolving Catalyst that Functions under Benign Conditions. *Proc. Natl. Acad. Sci. U. S. A.* **2010**, *107*, 10337–10341.

(11) Gardner, G. P.; Go, Y. B.; Robinson, D. M.; Smith, P. F.; Hadermann, J.; Abakumov, A.; Greenblatt, M.; Dismukes, G. C. Structural Requirements in Lithium Cobalt Oxides for the Catalytic Oxidation of Water. *Angew. Chem., Int. Ed.* **2012**, *51*, 1616–1619.

(12) Barnett, S. M.; Goldberg, K. I.; Mayer, J. M. A Soluble Copper-Bipyridine Water-Oxidation Electrocatalyst. *Nat. Chem.* **2012**, *4*, 498–502.

(13) Cobo, S.; Heidkamp, J.; Jacques, P. A.; Fize, J.; Fourmond, V.; Guetaz, L.; Jousselme, B.; Ivanova, V.; Dau, H.; Palacin, S.; Fontecave, M.; Artero, V. A Janus Cobalt-Based Catalytic Material for Electro-Splitting of Water. *Nat. Mater.* **2012**, *11*, 802–807.

(14) Zaharieva, I.; Chernev, P.; Risch, M.; Klingan, K.; Kohlhoff, M.; Fischer, A.; Dau, H. Electrosynthesis, Functional, and Structural Characterization of a Water-Oxidizing Manganese Oxide. *Energy Environ. Sci.* **2012**, *5*, 7081–7089.

(15) Smith, R. D. L.; Prévot, M. S.; Fagan, R. D.; Zhang, Z. P.; Sedach, P. A.; Siu, M. K. J.; Trudel, S.; Berlinguette, C. P. Photochemical Route for Accessing Amorphous Metal Oxide Materials for Water Oxidation Catalysis. *Science* **2013**, *340*, 60–63.

(16) Pintado, S.; Goberna-Ferrón, S.; Escudero-Adán, E. C.; Galán-Mascarós, J. R. Fast and Persistent Electrocatalytic Water Oxidation by Co-Fe Prussian Blue Coordination Polymers. *J. Am. Chem. Soc.* **2013**, *135*, 13270–13273.

(17) Zhou, X.; Zhang, T.; Abney, C. W.; Li, Z.; Lin, W. B. Graphene-Immobilized Monomeric Bipyridine-M^{x+} (M^{x+} = Fe^{3+}, Co^{2+}, Ni^{2+}, or Cu^{2+}) Complexes for Electrocatalytic Water Oxidation. *ACS Appl. Mater. Interfaces* **2014**, *6*, 18475–18479.

(18) Zhao, P.; Koel, B. E. Water Oxidation Catalysis: Effects of Nickel Incorporation on the Structural and Chemical Properties of the α-Fe_2O_3(0001) Surface. *ACS Appl. Mater. Interfaces* **2014**, *6*, 22289–22296.

(19) Lei, H. T.; Han, A. L.; Li, F. W.; Zhang, M. N.; Han, Y. Z.; Du, P. W.; Lai, W. Z.; Cao, R. Electrochemical, Spectroscopic and Theoretical Studies of a Simple Bifunctional Cobalt Corrole Catalyst for Oxygen Evolution and Hydrogen Production. *Phys. Chem. Chem. Phys.* **2014**, *16*, 1883–1893.

(20) Lu, X. Y.; Zhao, C. Electrodeposition of Hierarchically Structured Three-Dimensional Nickel-Iron Electrodes for Efficient Oxygen Evolution at High Current Densities. *Nat. Commun.* **2015**, *6*, 6616.

(21) Zhou, T. H.; Wang, D. P.; Goh, S. C. K.; Hong, J. D.; Han, J. Y.; Mao, J. G.; Xu, R. Bio-Inspired Organic Cobalt(II) Phosphonates toward Water Oxidation. *Energy Environ. Sci.* **2015**, *8*, 526–534.

(22) Concepcion, J. J.; Jurss, J. W.; Brennaman, M. K.; Hoertz, P. G.; Patrocinio, A. O. T.; Iha, N. Y. M.; Templeton, J. L.; Meyer, T. J. Making Oxygen with Ruthenium Complexes. *Acc. Chem. Res.* **2009**, *42*, 1954–1965.

(23) Chen, Z. F.; Concepcion, J. J.; Hu, X. Q.; Yang, W. T.; Hoertz, P. G.; Meyer, T. J. Concerted O Atom-Proton Transfer in the O-O Bond Forming Step in Water Oxidation. *Proc. Natl. Acad. Sci. U. S. A.* **2010**, *107*, 7225–7229.

(24) Polyansky, D. E.; Muckerman, J. T.; Rochford, J.; Zong, R. F.; Thummel, R. P.; Fujita, E. Water Oxidation by a Mononuclear Ruthenium Catalyst: Characterization of the Intermediates. *J. Am. Chem. Soc.* **2011**, *133*, 14649–14665.

(25) Duan, L. L.; Fischer, A.; Xu, Y. H.; Sun, L. C. Isolated Seven-Coordinate Ru(IV) Dimer Complex with $[HOHOH]^-$ Bridging Ligand as an Intermediate for Catalytic Water Oxidation. *J. Am. Chem. Soc.* **2009**, *131*, 10397–10399.

(26) Duan, L. L.; Bozoglian, F.; Mandal, S.; Stewart, B.; Privalov, T.; Llobet, A.; Sun, L. C. A Molecular Ruthenium Catalyst with Water-Oxidation Activity Comparable to that of Photosystem II. *Nat. Chem.* **2012**, *4*, 418–423.

(27) McDaniel, N. D.; Coughlin, F. J.; Tinker, L. L.; Bernhard, S. Cyclometalated Iridium(III) Aquo Complexes: Efficient and Tunable Catalysts for the Homogeneous Oxidation of Water. *J. Am. Chem. Soc.* **2008**, *130*, 210–217.

DOI: 10.1021/acsami.5b06195
ACS Appl. Mater. Interfaces 2015, 7, 21852–21859

(28) deKrafft, K. E.; Wang, C.; Xie, Z. G.; Su, X.; Hinds, B. J.; Lin, W. B. Electrochemical Water Oxidation with Carbon-Grafted Iridium Complexes. *ACS Appl. Mater. Interfaces* **2012**, *4*, 608−613.
(29) Hu, W.; Zhong, H. W.; Liang, W.; Chen, S. L. Ir-Surface Enriched Porous Ir-Co Oxide Hierarchical Architecture for High Performance Water Oxidation in Acidic Media. *ACS Appl. Mater. Interfaces* **2014**, *6*, 12729−12736.
(30) Lattach, Y.; Rivera, J. F.; Bamine, T.; Deronzier, A.; Moutet, J. C. Iridium Oxide-Polymer Nanocomposite Electrode Materials for Water Oxidation. *ACS Appl. Mater. Interfaces* **2014**, *6*, 12852−12859.
(31) Liang, Y. Y.; Li, Y. G.; Wang, H. L.; Zhou, J. G.; Wang, J.; Regier, T.; Dai, H. J. Co_3O_4 Nanocrystals on Graphene as a Synergistic Catalyst for Oxygen Reduction Reaction. *Nat. Mater.* **2011**, *10*, 780−786.
(32) Miao, C. H.; Ji, S. L.; Xu, G. P.; Liu, G. D.; Zhang, L. D.; Ye, C. H. Micro-Nano-Structured Fe_2O_3:Ti/$ZnFe_2O_4$ Heterojunction Films for Water Oxidation. *ACS Appl. Mater. Interfaces* **2012**, *4*, 4428−4433.
(33) Jun, K.; Lee, Y. S.; Buonassisi, T.; Jacobson, J. M. High Photocurrent in Silicon Photoanodes Catalyzed by Iron Oxide Thin Films for Water Oxidation. *Angew. Chem., Int. Ed.* **2012**, *51*, 423−427.
(34) Landon, J.; Demeter, E.; İnoğlu, N.; Keturakis, C.; Wachs, I. E.; Vasić, R.; Frenkel, A. I.; Kitchin, J. R. Spectroscopic Characterization of Mixed Fe-Ni Oxide Electrocatalysts for the Oxygen Evolution Reaction in Alkaline Electrolytes. *ACS Catal.* **2012**, *2*, 1793−1801.
(35) Singh, A.; Chang, S. L. Y.; Hocking, R. K.; Bach, U.; Spiccia, L. Highly Active Nickel Oxide Water Oxidation Catalysts Deposited from Molecular Complexes. *Energy Environ. Sci.* **2013**, *6*, 579−586.
(36) Smith, R. D. L.; Prévot, M. S.; Fagan, R. D.; Trudel, S.; Berlinguette, C. P. Water Oxidation Catalysis: Electrocatalytic Response to Metal Stoichiometry in Amorphous Metal Oxide Films Containing Iron, Cobalt, and Nickel. *J. Am. Chem. Soc.* **2013**, *135*, 11580−11586.
(37) Zandi, O.; Klahr, B. M.; Hamann, T. W. Highly Photoactive Ti-Doped α-Fe_2O_3 Thin Film Electrodes: Resurrection of the Dead Layer. *Energy Environ. Sci.* **2013**, *6*, 634−642.
(38) Bora, D. K.; Braun, A.; Constable, E. C. "In Rust We Trust". Hematite-the Prospective Inorganic Backbone for Artificial Photosynthesis. *Energy Environ. Sci.* **2013**, *6*, 407−425.
(39) Liao, L.; Zhang, Q. H.; Su, Z. H.; Zhao, Z. Z.; Wang, Y. N.; Li, Y.; Lu, X. X.; Wei, D. G.; Feng, G. Y.; Yu, Q. K.; Cai, X. J.; Zhao, J. M.; Ren, Z. F.; Fang, H.; Robles-Hernandez, F.; Baldelli, S.; Bao, J. M. Efficient Solar Water-Splitting Using a Nanocrystalline CoO Photocatalyst. *Nat. Nanotechnol.* **2014**, *9*, 69−73.
(40) Gerken, J. B.; Shaner, S. E.; Massé, R. C.; Porubsky, N. J.; Stahl, S. S. A Survey of Diverse Earth Abundant Oxygen Evolution Electrocatalysts Showing Enhanced Activity from Ni-Fe Oxides Containing a Third Metal. *Energy Environ. Sci.* **2014**, *7*, 2376−2382.
(41) Chen, S. S.; Shen, S.; Liu, G. J.; Qi, Y.; Zhang, F. X.; Li, C. Interface Engineering of a CoO_x/Ta_3N_5 Photocatalyst for Unprecedented Water Oxidation Performance under Visible-Light-Irradiation. *Angew. Chem., Int. Ed.* **2015**, *54*, 3047−3051.
(42) Singh, S. K.; Dhavale, V. M.; Kurungot, S. Low Surface Energy Plane Exposed Co_3O_4 Nanocubes Supported on Nitrogen-Doped Graphene as an Electrocatalyst for Efficient Water Oxidation. *ACS Appl. Mater. Interfaces* **2015**, *7*, 442−451.
(43) Chen, S.; Duan, J. J.; Jaroniec, M.; Qiao, S. Z. Three-Dimensional N-Doped Graphene Hydrogel/NiCo Double Hydroxide Electrocatalysts for Highly Efficient Oxygen Evolution. *Angew. Chem., Int. Ed.* **2013**, *52*, 13567−13570.
(44) Gong, M.; Li, Y. G.; Wang, H. L.; Liang, Y. Y.; Wu, J. Z.; Zhou, J. G.; Wang, J.; Regier, T.; Wei, F.; Dai, H. J. An Advanced Ni-Fe Layered Double Hydroxide Electrocatalyst for Water Oxidation. *J. Am. Chem. Soc.* **2013**, *135*, 8452−8455.
(45) Gao, M. R.; Sheng, W. C.; Zhuang, Z. B.; Fang, Q. R.; Gu, S.; Jiang, J.; Yan, Y. S. Efficient Water Oxidation Using Nanostructured α-Nickel-Hydroxide as an Electrocatalyst. *J. Am. Chem. Soc.* **2014**, *136*, 7077−7084.
(46) Seabold, J. A.; Choi, K. S. Efficient and Stable Photo-Oxidation of Water by a Bismuth Vanadate Photoanode Coupled with an Iron Oxyhydroxide Oxygen Evolution Catalyst. *J. Am. Chem. Soc.* **2012**, *134*, 2186−2192.
(47) Louie, M. W.; Bell, A. T. An Investigation of Thin-Film Ni-Fe Oxide Catalysts for the Electrochemical Evolution of Oxygen. *J. Am. Chem. Soc.* **2013**, *135*, 12329−12337.
(48) Chemelewski, W. D.; Lee, H. C.; Lin, J. F.; Bard, A. J.; Mullins, C. B. Amorphous FeOOH Oxygen Evolution Reaction Catalyst for Photoelectrochemical Water Splitting. *J. Am. Chem. Soc.* **2014**, *136*, 2843−2850.
(49) Trotochaud, L.; Young, S. L.; Ranney, J. K.; Boettcher, S. W. Nickel-Iron Oxyhydroxide Oxygen-Evolution Electrocatalysts: The Role of Intentional and Incidental Iron Incorporation. *J. Am. Chem. Soc.* **2014**, *136*, 6744−6753.
(50) Han, Y. Z.; Wu, Y. Z.; Lai, W. Z.; Cao, R. Electrocatalytic Water Oxidation by a Water-Soluble Nickel Porphyrin Complex at Neutral pH with Low Overpotential. *Inorg. Chem.* **2015**, *54*, 5604−5613.
(51) Wu, Y. Z.; Chen, M. X.; Han, Y. Z.; Luo, H. X.; Su, X. J.; Zhang, M.-T.; Lin, X. H.; Sun, J. L.; Wang, L.; Deng, L.; Zhang, W.; Cao, R. Fast and Simple Preparation of Iron-Based Thin Films as Highly Efficient Water-Oxidation Catalysts in Neutral Aqueous Solution. *Angew. Chem., Int. Ed.* **2015**, *54*, 4870−4875.
(52) Tshuva, E. Y.; Lippard, S. J. Synthetic Models for Non-Heme Carboxylate-Bridged Diiron Metalloproteins: Strategies and Tactics. *Chem. Rev.* **2004**, *104*, 987−1011.
(53) Denisov, I. G.; Makris, T. M.; Sligar, S. G.; Schlichting, I. Structure and Chemistry of Cytochrome P450. *Chem. Rev.* **2005**, *105*, 2253−2277.
(54) Kanan, M. W.; Surendranath, Y.; Nocera, D. G. Cobalt-Phosphate Oxygen-Evolving Compound. *Chem. Soc. Rev.* **2009**, *38*, 109−114.
(55) Bediako, D. K.; Lassalle-Kaiser, B.; Surendranath, Y.; Yano, J.; Yachandra, V. K.; Nocera, D. G. Structure-Activity Correlations in a Nickel-Borate Oxygen Evolution Catalyst. *J. Am. Chem. Soc.* **2012**, *134*, 6801−6809.
(56) Singh, A.; Chang, S. L. Y.; Hocking, R. K.; Bach, U.; Spiccia, L. Anodic Deposition of NiO_x Water Oxidation Catalysts from Macrocyclic Nickel(II) Complexes. *Catal. Sci. Technol.* **2013**, *3*, 1725−1732.
(57) Zhang, Y.; Cui, B.; Zhao, C. S.; Lin, H.; Li, J. B. Co-Ni Layered Double Hydroxides for Water Oxidation in Neutral Electrolyte. *Phys. Chem. Chem. Phys.* **2013**, *15*, 7363−7369.
(58) Trotochaud, L.; Ranney, J. K.; Williams, K. N.; Boettcher, S. W. Solution-Cast Metal Oxide Thin Film Electrocatalysts for Oxygen Evolution. *J. Am. Chem. Soc.* **2012**, *134*, 17253−17261.
(59) Kuai, L.; Geng, J.; Chen, C. Y.; Kan, E. J.; Liu, Y. D.; Wang, Q.; Geng, B. Y. A Reliable Aerosol-Spray-Assisted Approach to Produce and Optimize Amorphous Metal Oxide Catalysts for Electrochemical Water Splitting. *Angew. Chem., Int. Ed.* **2014**, *53*, 7547−7551.
(60) Xiao, C. L.; Lu, X. Y.; Zhao, C. Unusual Synergistic Effects upon Incorporation of Fe and/or Ni into Mesoporous Co_3O_4 for Enhanced Oxygen Evolution. *Chem. Commun.* **2014**, *50*, 10122−10125.
(61) Chen, J. Y. C.; Miller, J. T.; Gerken, J. B.; Stahl, S. S. Inverse Spinel $NiFeAlO_4$ as a Highly Active Oxygen Evolution Electrocatalyst: Promotion of Activity by a Redox-Inert Metal Ion. *Energy Environ. Sci.* **2014**, *7*, 1382−1386.
(62) Fan, C. L.; Piron, D. L. Electrodeposition as a Means of Producing Large-Surface Electrodes Required in Water Electrolysis. *Surf. Coat. Technol.* **1995**, *73*, 91−97.
(63) Surendranath, Y.; Dincă, M.; Nocera, D. G. Electrolyte-Dependent Electrosynthesis and Activity of Cobalt-Based Water Oxidation Catalysts. *J. Am. Chem. Soc.* **2009**, *131*, 2615−2620.
(64) Bergmann, A.; Zaharieva, I.; Dau, H.; Strasser, P. Electrochemical Water Splitting by Layered and 3D Cross-Linked Manganese Oxides: Correlating Structural Motifs and Catalytic Activity. *Energy Environ. Sci.* **2013**, *6*, 2745−2755.
(65) Jin, K.; Park, J.; Lee, J.; Yang, K. D.; Pradhan, G. K.; Sim, U.; Jeong, D.; Jang, H. L.; Park, S.; Kim, D.; Sung, N. E.; Kim, S. H.; Han, S.; Nam, K. T. Hydrated Manganese(II) Phosphate ($Mn_3(PO_4)_2$·

DOI: 10.1021/acsami.5b06195
ACS Appl. Mater. Interfaces 2015, 7, 21852−21859

$3H_2O$) as a Water Oxidation Catalyst. *J. Am. Chem. Soc.* **2014**, *136*, 7435−7443.
(66) Jeong, D.; Jin, K.; Jerng, S. E.; Seo, H.; Kim, D.; Nahm, S. H.; Kim, S. H.; Nam, K. T. Mn_5O_8 Nanoparticles as Efficient Water Oxidation Catalysts at Neutral pH. *ACS Catal.* **2015**, *5*, 4624−4628.
(67) Fekete, M.; Hocking, R. K.; Chang, S. L. Y.; Italiano, C.; Patti, A. F.; Arena, F.; Spiccia, L. Highly Active Screen-Printed Electrocatalysts for Water Oxidation Based on β-Manganese Oxide. *Energy Environ. Sci.* **2013**, *6*, 2222−2232.
(68) Yamaguchi, A.; Inuzuka, R.; Takashima, T.; Hayashi, T.; Hashimoto, K.; Nakamura, R. Regulating Proton-Coupled Electron Transfer for Efficient Water Splitting by Manganese Oxides at Neutral pH. *Nat. Commun.* **2014**, *5*, 4256.
(69) Park, J.; Kim, H.; Jin, K.; Lee, B. J.; Park, Y. S.; Kim, H.; Park, I.; Yang, K. D.; Jeong, H. Y.; Kim, J.; Hong, K. T.; Jang, H. W.; Kang, K.; Nam, K. T. A New Water Oxidation Catalyst: Lithium Manganese Pyrophosphate with Tunable Mn Valency. *J. Am. Chem. Soc.* **2014**, *136*, 4201−4211.
(70) Ramírez, A.; Bogdanoff, P.; Friedrich, D.; Fiechter, S. Synthesis of $Ca_2Mn_3O_8$ Films and Their Electrochemical Studies for the Oxygen Evolution Reaction (OER) of Water. *Nano Energy* **2012**, *1*, 282−289.
(71) Chen, Z. F.; Rathmell, A. R.; Ye, S. R.; Wilson, A. R.; Wiley, B. J. Optically Transparent Water Oxidation Catalysts Based on Copper Nanowires. *Angew. Chem., Int. Ed.* **2013**, *52*, 13708−13711.
(72) Du, J. L.; Chen, Z. F.; Ye, S. R.; Wiley, B. J.; Meyer, T. J. Copper as a Robust and Transparent Electrocatalyst for Water Oxidation. *Angew. Chem., Int. Ed.* **2015**, *54*, 2073−2078.
(73) Fominykh, K.; Feckl, J. M.; Sicklinger, J.; Döblinger, M.; Böcklein, S.; Ziegler, J.; Peter, L.; Rathousky, J.; Scheidt, E. W.; Bein, T.; Fattakhova-Rohlfing, D. Ultrasmall Dispersible Crystalline Nickel Oxide Nanoparticles as High-Performance Catalysts for Electrochemical Water Splitting. *Adv. Funct. Mater.* **2014**, *24*, 3123−3129.
(74) Yeo, B. S.; Bell, A. T. Enhanced Activity of Gold-Supported Cobalt Oxide for the Electrochemical Evolution of Oxygen. *J. Am. Chem. Soc.* **2011**, *133*, 5587−5593.
(75) Gorlin, Y.; Chung, C. J.; Benck, J. D.; Nordlund, D.; Seitz, L.; Weng, T. C.; Sokaras, D.; Clemens, B. M.; Jaramillo, T. F. Understanding Interactions between Manganese Oxide and Gold That Lead to Enhanced Activity for Electrocatalytic Water Oxidation. *J. Am. Chem. Soc.* **2014**, *136*, 4920−4926.
(76) Lim, B.; Jiang, M. J.; Camargo, P. H. C.; Cho, E. C.; Tao, J.; Lu, X. M.; Zhu, Y. M.; Xia, Y. N. Pd-Pt Bimetallic Nanodendrites with High Activity for Oxygen Reduction. *Science* **2009**, *324*, 1302−1305.
(77) Shao, Y. Y.; Zhang, S.; Engelhard, M. H.; Li, G. S.; Shao, G. C.; Wang, Y.; Liu, J.; Aksay, I. A.; Lin, Y. H. Nitrogen-Doped Graphene and Its Electrochemical Applications. *J. Mater. Chem.* **2010**, *20*, 7491−7496.
(78) Abidat, I.; Bouchenafa-Saib, N.; Habrioux, A.; Comminges, C.; Canaff, C.; Rousseau, J.; Napporn, T. W.; Dambournet, D.; Borkiewicz, O.; Kokoh, K. B. Electrochemically Induced Surface Modifications of Mesoporous Spinels ($Co_3O_{4-\delta}$, $MnCo_2O_{4-\delta}$, $NiCo_2O_{4-\delta}$) as the Origin of the OER Activity and Stability in Alkaline Medium. *J. Mater. Chem. A* **2015**, *3*, 17433−17444.
(79) Kim, T. J.; Kwon, G.; Kim, Y. T. Anomalously Increased Oxygen Reduction Reaction Activity with Accelerated Durability Test Cycles for Platinum on Thiolated Carbon Nanotubes. *Chem. Commun.* **2014**, *50*, 596−598.
(80) Sun, S. H.; Zhang, G. X.; Geng, D. S.; Chen, Y. G.; Li, R. Y.; Cai, M.; Sun, X. L. A Highly Durable Platinum Nanocatalyst for Proton Exchange Membrane Fuel Cells: Multiarmed Starlike Nanowire Single Crystal. *Angew. Chem., Int. Ed.* **2011**, *50*, 442−426.
(81) Moulder, J. F.; Stickle, W. F.; Sobol, P. E.; Bomben, K. D. *Handbook of X-ray Photoelectron Spectroscopy*. Perkin Elmer, Eden Prairie, MN, 1992.

DOI: 10.1021/acsami.5b06195
ACS Appl. Mater. Interfaces 2015, 7, 21852−21859